Solar-powered Seesaw Extractor ~~Boosts~~ for Lithium ~~Extraction~~ Production from Seawater

Yi-Zhou Chen[1,2], Hao-Nan Li[1,2], Jia-Hui Xin[1,2], Ling-Shu Wan[1,2], Hao-Cheng Yang[1,2], Seth B Darling[4,5*], Zhi-Kang Xu[1,2,3*]*

[1]MOE Key Laboratory of Macromolecular Synthesis and Functionalization, Key Laboratory of Adsorption and Separation Materials & Technologies of Zhejiang Province, Department of Polymer Science and Engineering, Zhejiang University; Hangzhou, 310058, P. R. China.

[2]The "Belt and Road" Sino-Portugal Joint Lab on Advanced Materials, International Research Center for X Polymers, Zhejiang University; Hangzhou, 310058, P. R. China.

[3]Institute of Marine Chemistry and Environment, Ocean College, Zhejiang University; Zhoushan, 316021, P. R. China.

[4] Center for Molecular Engineering, Chemical Sciences and Engineering Division and Advanced Materials for Energy-Water Systems (AMEWS) Energy Frontier Research Center, Argonne National Laboratory, Lemont, IL 60439, USA

[5] Pritzker School of Molecular Engineering, University of Chicago, Chicago, IL 60637, USA

Keywords: solar-powered lithium extraction, seawater, seesaw extractor, localized enrichment, self-descaling

Commented [A1]: Authors are encouraged to include their native names in ( ).

Abstract

~~Extracting lithium from seawater offers a promising solution to meet the growing demand for lithium ion batteries. However, the extremely~~The low Li^+ concentration and the abundance of competing ions ~~severely~~ limit the efficiency of lithium ~~existing~~ extraction in seawater ~~technologies~~. ~~We~~ In this work, we report a solar-powered seesaw extractor (SPSE) to boost Li^+ adsorption while minimizing scaling caused by competing ions during photothermal evaporation. The SPSE features a sandwich architecture, with a hydrophilic adsorbent layer ~~sandwiched~~ placed between two hydrophobic photothermal layers. The seesaw configuration enables Li^+ to be elevated and concentrated ~~rapidly~~ through evaporation to overcome sluggish adsorption kinetics, while the associated salt scaling is removed by the s~~elf rocking~~eesawing motion. ~~SPSEs~~ As demonstration, we ~~are~~ assembled SPSEs into ~~arrays~~ an array that achieve a 15.5-fold increase in local Li^+ concentration and a 69.1% improvement in Li^+ uptake over 120 hours, with a Li^+/Na^+ separation factor exceeding 370,000.

Commented [A2]: How many by how many?

Introduction

~~Lithium~~ The ~~is a crucial component in lithium-ion batteries, with~~ global demand for lithium is projected to increase six-fold from 2020 to 2030 due to the rise of various electric vehicles and mobile devices [1-4]. ~~Lithium resources in the terrestrial parts of the world are projected to be depleted by 2050 [5].~~ Seawater is an abundant source for lithium, ~~,~~ containing approximately 230 billion tons of lithium~~, presents a potential supplementary source~~ [6]. However, the high level of competing ions, such as Na^+ (exceeding 12,000 $mg \cdot L^{-1}$), limits the ~~direct~~ efficiency of ~~application of~~ lithium extraction ~~technologies from brines to seawater~~techniques[7], ~~including~~ such as electrochemical intercalation[8,9], nanofiltration-enabled separation [10] and liquid-liquid extraction [11]. Lithium-ion sieves such as hydrogen manganese oxide (HMO) ~~stand out for their exceptional selectivity~~may have the necessary selectivity, but are restricted by sluggish adsorption kinetics under ~~extremely~~ the low concentration of Li^+ in seawater (around 0.2 $mg \cdot L^{-1}$) [12,13]. Interfacial evaporation has been integrated with lithium-ion sieves to enhance the local enrichment and adsorption thermodynamics [14-19]~~. Unfortunately~~, but the ~~concurrent~~ enrichment of other ions leads to scaling before reaching sufficient Li^+ levels for effective adsorption. This scaling ~~not only~~ hinders interfacial evaporation and ~~but also~~ obstructs Li^+ diffusion to the adsorption sites [15,16,20,21].

~~To address these challenges, it is crucial to develop an extraction system that enables efficient local enrichment while mitigating scaling issues. Herein,~~ In this work, we ~~propose~~ present a solar-powered seesaw extractor (SPSE) for ~~rapid and durable~~ Li^+ ~~extraction~~ production from seawater **(Figure 1)**. This extractor features a hydrophilic HMO-loaded nanofibrous mat sandwiched between two hydrophobic carbon paper layers. In a seesaw configuration, interfacial evaporation by the carbon paper induces water to ~~continuously~~ flow and pump Li^+ into the nanofibrous mat for achieving an ~~maximum~~ enrichment of 15.5-fold. This strategy ~~significantly~~ enhances the Li^+

Commented [A3]: Possible to just give a number for 2030?

Commented [A4]: Where is the original source for this statement? The cited reference here is a review.

Commented [A5]: Some references are removed during edits. Please review and update as needed.

adsorption kinetics of the loaded HMO. Moreover, the scaling of competing ions, alongside Li^+ adsorption, triggers the self-rocking of the SPSE once a ~~specific~~ threshold is reached. This process re-dissolves the scale into seawater and facilitates exclusive Li^+ extraction. ~~Therefore,~~ ~~t~~The SPSE ~~array~~ achieves a Li^+/Na^+ separation factor exceeding 370,000, with a Li^+ uptake rate of up to ~~nearly~~ 2.5 $mg \cdot g^{-1}$HMO$\cdot day^{-1}$ from simulated seawater over three days of exposure to natural sunlight.

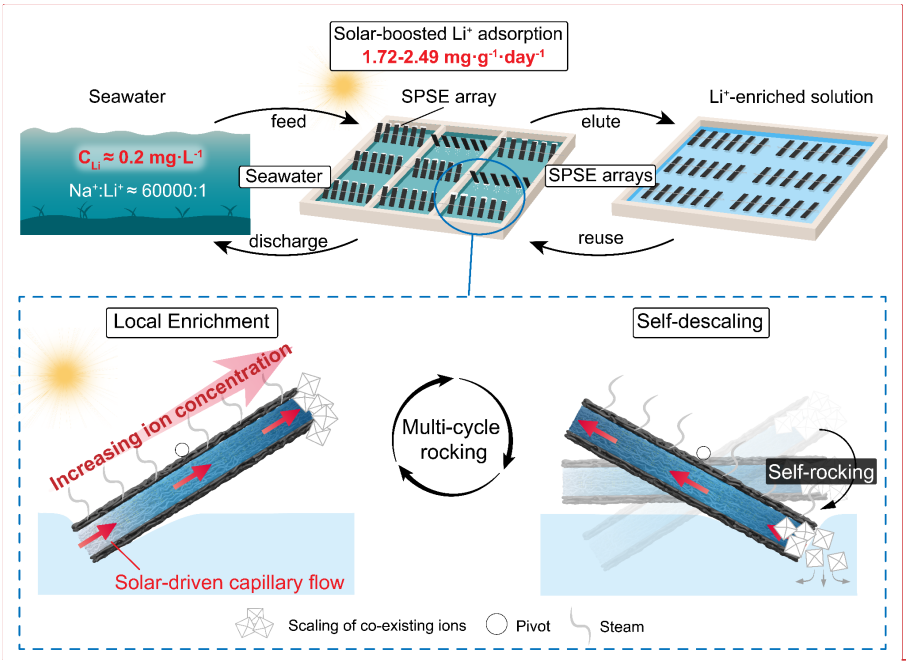

Figure 1. Principles of Li^+ extraction from seawater by SPSEs. The synergistic effects of enrichment and self-descaling enable SPSEs to efficiently extract Li^+ from seawater. The increased local concentration of Li^+ overcomes the slow adsorption kinetics, while self-descaling allows the scale of coexisting ions to redissolve into the seawater.

Results ~~and Discussion~~

Commented [A6]: Why not use real seawater here?

Commented [A7]: (1) When you revise, please remove all images from the main document and upload them to our system as individual image files.

(2) Then, please move the captions to the bottom of the main text (after references)

Design of SPSE for Ion Enrichment from Seawater

The SPSE consists of a tri-layer structure, with a hydrophilic adsorption mat made of polyacrylonitrile (PAN)/HMO composite nanofibers sandwiched between two hydrophobic carbon paper layers **(Figure 2a)**. ~~It is worth noting that both t~~The carbon paper and PAN ~~are selected for their excellent stability. These materials~~ maintain structural stability under UV irradiation and high-salinity conditions, thereby endowing the SPSE with ~~strong long-term~~ stability for outdoor applications. The composite nanofibers were electrospun from PAN solution with added HMO nanoparticles. These nanofibers have an average diameter of 914 ± 168 nm uniformly distributed with 44.3 wt% of HMO nanoparticles **(Figure 2b)**. Most of the HMO nanoparticles are exposed on the surface of the nanofibers, resulting in an ~~effective~~ adsorption capacity of 90.1% compared to HMO powders (Figure S1). The as-prepared nanofibers were folded and hot-pressed to gain a mat with desired thickness (Figure S2). In the SPSE, the hydrophilic nanofibrous mat functions as both a capillary pump for ion transport and a reservoir for Li^+ capture. It ~~can is~~be ~~rapidly~~ filled with water through capillary flow, enabling continuous ion transport alongside evaporation (Figure S3). ~~In addition, t~~The upper carbon paper converts light into heat for evaporation, ~~while~~ and the lower carbon paper enables the extractor to float on the water surface and reduces the dragging force from the liquid bridge (Figure S4-S5) [22]. The hydrophobic layers ~~also~~ help ~~to~~ direct the salt deposition ~~primarily~~ to the edges of the SPSE, mitigating ~~the impact of~~ scaling on evaporation before rocking.

The seesaw configuration plays a critical role in the ~~rapid~~ enrichment of Li^+ during evaporation, as the ions ~~continuously~~ accumulate at the upper end of the SPSE. The ion accumulation arises from the competition between evaporation-driven flow and back-diffusion. **Figure 2c** depicts the evaporation rates of SPSE at varying tilt angles, which leads to inner

Commented [A8]: Stability in what?

advection within the SPSE. The SPSE at 0° represents ~~the~~ a ~~conventional~~ floating configuration~~,~~ ~~which~~ without~~lacks~~ the bottom carbon paper layer. The Peclet number $P_e = Lu/D_{ion}$ quantifies the competition between advection and diffusion, where L, u and D_{ion} represent characteristic length, characteristic flow velocity, and ion mass diffusivity, respectively. In the seesaw configuration, a ~~relatively~~ larger L leads to dominant advection, whereas diffusion predominates in the floating configuration **(Figure 2d)**. This leads to greater ion accumulation in the seesaw configuration, whereas ions diffuse back in the floating configuration. As the results, the enrichment of ions in the floating configuration is lower than that observed in the seesaw configuration under different tilt angles (Figure S6). Besides, the enrichment of ions within the SPSE increases as evaporation progresses, creating a concentration gradient along the device (Figure S7). **Figure 2e** compares the concentration distribution after 10 hours of evaporation with the simulation results. The enrichment relative to the initial concentration reaches 3.1, 8.2, 10.5, and 15.5×, from the bottom to the top, respectively, consistent with ~~the~~ simulated values.

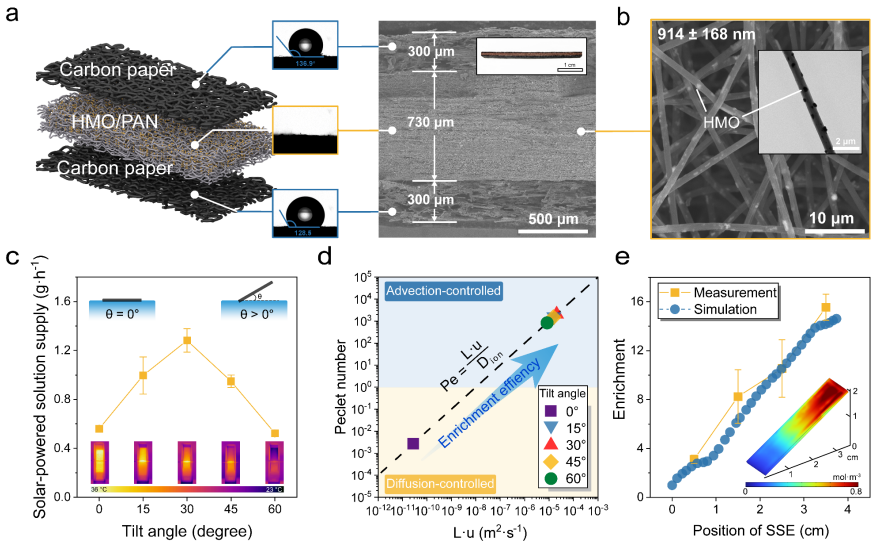

Commented [A9]: ?? The bottom layer isn't present with the SPSE is at 0 deg?

Commented [A10]: Meaning tilted? A seesaw would imply a moving object. Please make sure that the correct descriptor is used throughout the main text, for seesaw (moving) vs tilted (static).

Formatted: Highlight

Formatted: Highlight

Figure 2. Materials design and enrichment effect of SPSEs. (a) Cross-section morphology of the SPSE, which consists of a hydrophilic adsorption layer sandwiched between two hydrophobic carbon paper layers. (b) SEM and TEM images show that HMO nanoparticles are uniformly distributed within nanofibers. (c) Solar-powered solution supply of SPSEs at different tilt angles. The inserted thermal images show the surface temperature of SPSEs during evaporation. (d) Peclet numbers of SPSEs at different tilt angles. Advection dominates the transport process when the Peclet number is larger than 1, otherwise, the transport process is governed by ion diffusion. (e) Enrichment of ions within the SPSE. The insert is the simulation of the ion concentration distribution within the SPSE.

Li^+ adsorption kinetics in SPSE

~~Conventional~~ Li^+ adsorption from seawater is hindered by the kinetic trap resulting from the ~~extremely~~ low Li^+ concentration, which can be alleviated through the enrichment effect mentioned above. The tilt angle of the seesaw configuration ~~i~~as a crucial parameter ~~governs~~of the enrichment ~~degree, thereby exerting a significant influence on the Li^+ adsorption capacity~~. The Li^+ adsorption capacity of SPSE at ~~an ultra-low Li^+ concentration (~~0.4 $mg \cdot L^{-1}$~~)~~ initially increases with tilt angles, then decreases, corresponding to the ion enrichment observed above (Figure S8). The highest Li^+ adsorption capacity is achieved at 30°. Considering the solution supply, 30° was selected as the tilt angle of seesaw configuration for subsequent tests. ~~Then, w~~

We compared the Li^+ adsorption capacity of the extractor in two modes: immersion mode and seesaw mode, each over 24 hours~~,~~ with varying initial Li^+ concentrations **(Figure 3a)**. In immersion mode, the extractor is fully submerged in water, whereas in seesaw mode, it is positioned as a seesaw. At a relatively low Li^+ concentration (<0.4 $mg \cdot L^{-1}$), the seesaw mode outperforms the immersion mode, presenting increases in adsorption capacity of 67.3% and 45.1%

Commented [A11]: And tilting? Can this sentence be combined with the next one to help transition the discussion?

Commented [A12]: Where above (in addition to Fig. S8)?

Commented [A13]: How much of it is submerged and how much is not?

at concentrations of 0.2 mg·L^{-1} and 0.4 mg·L^{-1}, respectively. ~~In contrast, w~~When the Li^+ concentration increases to 250 mg·L^{-1}, the seesaw mode becomes less efficient than the immersion mode due to the increased mass transfer distance~~, which emerges as the dominant limiting factor at a higher Li^+ concentration~~. ~~These results suggest that the SPSE is particularly effective in low-concentration sources, such as seawater and reverse osmosis brine.~~

The adsorption kinetics were ~~further~~ investigated at a Li^+ concentration of 0.4 mg·L^{-1}, which is a representative of the typical Li^+ concentration in seawater reverse osmosis brine **(Figure 3b)**. Within the initial 4 h, the immersion mode exhibits an ~~competitive~~ adsorption rate ~~compared~~ comparable to the seesaw mode. Then, it experiences a ~~relatively~~ slower adsorption stage after 24 hours and reaches the adsorption equilibrium at 72 h. In contrast, the seesaw mode shows a continuous increase in adsorption capacity and does not~~, as it has not~~ yet reached the adsorption equilibrium at 120 h. After 120 hours of adsorption, the seesaw mode exhibits a Li^+ adsorption capacity of 2.99 mg·g^{-1}, compared to 1.77 mg·g^{-1} for the immersion mode, achieving a 69.1% enhancement.

The m~~M~~ixed-o~~O~~rder (MO) kinetic model [23], which can quantify the diffusion and adsorption respectively, was used to analyze the adsorption process of these two modes:

$$\frac{dq_t}{dt} = k_1'(q_e - q_t) + k_2'(q_e - q_t)^2 \quad (1)$$

~~Where~~ where q_t is the Li^+ adsorption capacity at time t (mg·g^{-1}), q_e is the equilibrium Li^+ adsorption capacity (mg·g^{-1}), k_1' is the pseudo-first-order rate constant (min^{-1}) and k_2' is the pseudo-second-order rate constant (g·mg^{-1}·min^{-1}). In the seesaw mode, k_1' (0.0219 min^{-1}) is higher than k_2' (0.0115 g·mg^{-1}·min^{-1}) during the 120 hours adsorption process, indicating that the adsorption process is primarily controlled by Li^+ diffusion. ~~In addition, the~~ The relatively low k_1'

(0.0187 min^{-1}) in the immersion mode indicates that the Li^+ diffusion rate is lower than that in the seesaw mode.

~~Based on these, t~~The diffusion of Li^+ ~~were~~ was further ~~further~~ analyzed by the Weber and Morris intraparticle diffusion model as described below [21]:

$$q_t = K_p t^{0.5} + C \quad (2)$$

where q_t is the Li^+ adsorption capacity at time t, K_p is the diffusion coefficient, and C is the diffusion constant. The linear fitting of the q_t-$t^{0.5}$ curve indicates the mass transfer process is controlled by ~~the following two steps:~~ external diffusion and internal diffusion **(Figure 3c)**. The diffusion coefficients for the first two steps in the seesaw mode ~~is~~are 0.455 and 0.291, respectively, compared to 0.301 and 0.153 in the immersion mode. ~~The result suggests that Li^+ diffuse faster within the seesaw mode compared to the immersion mode.~~ This enhanced diffusion behavior can be attributed to the evaporation-driven enrichment, which creates a concentration gradient that ~~persistently~~ drives Li^+ toward the adsorption sites~~.~~ and ~~The continuous Li^+ diffusion gradually~~ increases the adsorption capacity in the seesaw mode. I~~n contrast, i~~n the immersion mode, the adsorption capacity reaches equilibrium more quickly due to insufficient Li^+ diffusion. ~~More importantly, t~~The seesaw mode ~~also~~ demonstrated higher Li^+ extraction efficiency than the immersed mode ~~even~~ in ~~real~~ seawater collected from the Yellow Sea (120°18′ E, 35°82′ N), highlighting its robustness and applicability under realistic marine conditions (Figure S9).

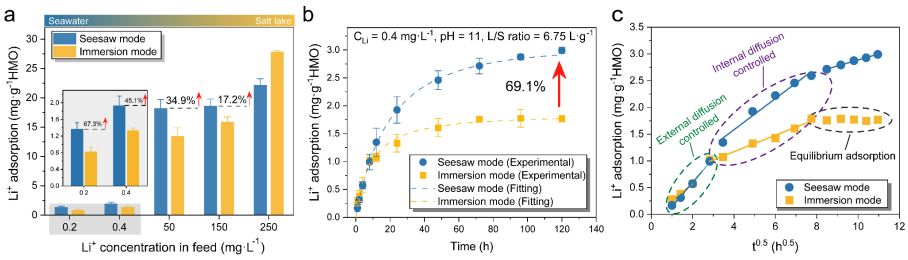

Formatted: Indent: First line: 0"

Formatted: Indent: First line: 0"

Figure 3. Li^+ extraction by SPSEs. (a) Li^+ adsorption capacity of SPSE in seesaw mode and immersion mode across various Li^+ concentrations. (b) Li^+ adsorption kinetics of seesaw mode and immersion mode in 0.4 $mg \cdot L^{-1}$ Li^+ solutions. The liquid/solid (L/S) ratio is 6.75 $L \cdot g^{-1}$, representing the ratio of the solution volume to the amount of HMO used. (c) Analysis of Li^+ diffusion kinetics within seesaw mode and immersion mode.

Self-descaling of SPSE

The competing ions are concentrated alongside ~~the target~~ Li^+, and can lead~~ing~~ to severe scaling during photothermal evaporation. Salt deposition ~~not only~~ obstructs light-to-heat conversion by covering the photothermal surface ~~but~~ and~~also~~ hinders Li^+ diffusion to adsorption sites by clogging the inner pores of HMO particles. The self-rocking motion of the seesaw ~~demonstrates~~ provides a ~~simple but effective~~ solution to mitigate these issues. The gravitational potential energy of salts converts to kinetic energy during this process. The ~~theoretical~~ required rocking ~~time~~ speed can be ~~estimated~~ calculated by measuring the torque required for ~~rocking~~ descaling (Figure S10-S1). For example, the SPSE flips position every 10 hours at a tilt angle of 30°. **Figure 4a** shows the ~~a typical~~ self-rocking process of the SPSE, in which the accumulated salt disrupts the force balance and triggers the action. The salts ~~rapidly~~ dissolve back into the ~~bulk~~ solution and the internal flow direction is ~~also~~ reversed, resulting in re-accumulation of the salt at the opposite end.

Figure 4b illustrates the variation in scaling mass during evaporation. The amount of salt on the SPSE increases linearly, with self-rocking occurring once the salt mass reaches 0.47 g. 86.3% of the accumulated scaling dissolves ~~rapidly~~ within 5 minutes, and the salt begins to accumulate linearly at the opposite end of the SPSE triggering the second self-rocking. As the tilt angle increased from 15° to 60°, the torque required to induce rocking ~~gradually~~ decreased, resulting in a reduction of the ~~critical~~ salt mass from 0.614 g to 0.240 g (Figure S12-13). These findings

Commented [A14]: Yes or no?

indicate that a larger tilt angle facilitates the onset of the self-rocking process by reducing the mechanical resistance associated with buoyancy and capillary adhesion. **Figure 4c** compares the long-term Li^+ adsorption of SPSE with and without rocking capacity.

The fitting curves of pseudo-second-order adsorption kinetics reveal a kinetic trap, attributed to the salt accumulation. The scaling-induced kinetic trap leads to a 22.6% reduction in the Li^+ adsorption capacity of the SPSE over a 120 ~~hour s~~hour adsorption process (Figure S14). The SPSE without rocking capacity exhibits a 43.3% decrease in solution supply compared to its initial state (Figure S15). The extractor becomes fully covered with ~~salts~~salt, which prevents ~~both~~ light absorption and water supply. ~~Additionally,~~ Ssalt~~s~~ is~~are~~ observed surrounding the HMO particles on the nanofibers because these inorganic particles can serve as heterogeneous nucleation sites for salt crystallization [24], which hinders Li^+ diffusion to the adsorption sites (Figure S16-17). Periodic self-rocking of the SPSE ~~effectively~~ mitigates the detrimental effects of ~~salt~~ scaling. ~~Moreover,~~ ~~t~~The self-rocking enables the ~~full~~ utilization of unabsorbed sites by reversing the ion transport direction (Figure S18). During the rocking cycles, Li^+ ions are captured by HMO and stored within the SPSE, while the salts dissolve back into the feed solution. As a result, Li^+ concentration decreases while the concentration of competing ions increases continuously over 120 hours **(Figure 4d)**.

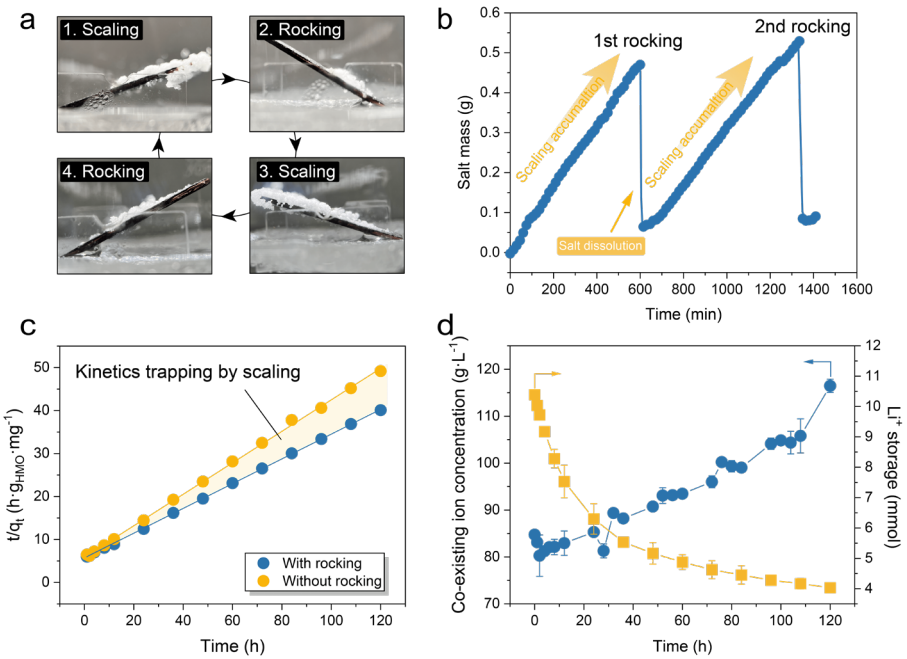

Figure 4. Self-rocking of the SPSE. (a) Digital images of the rocking processes. (b) Mass change of salt on the SPSE tilted at 30°over time. (c) Linear fitting plots of Li^+ adsorption by SPSEs with and without rocking using a pseudo-second-order model. (d) Variations in the concentration of ions in the bulk solution over time when SPSEs were employed to extract Li^+.

Li^+ extraction performance of SPSE

Separation factor ($S_{Li/M}$) is ~~utilized~~ used to evaluate the selectivity of SPSE in simulated seawater with an ultra-low Li^+/M^{n+} ratio. As shown in **Figure 5a**, the distribution coefficients (K_d) of different ions, including Li^+, Na^+, Mg^{2+}, K^+, and Ca^{2+}, between the SPSE and the simulated seawater are 1853, 0.005, 0.021, 0.011, and 0.383 $mL \cdot g^{-1}$, respectively, indicating ~~exceptional~~ selectivity of the SPSE towards Li^+. $S_{Li/Na}$ can achieve 376,332 and $S_{Li/Mg}$ can achieve 51,947,

surpassing previously reported values (**Figure 5b**, Figure S19, and Table S2). This ~~superior~~ selectivity arises from the synergistic effect of ion enrichment and self-rocking. The enrichment effect facilitates Li^+ adsorption by HMO, while coexisting ions tend to form salt crystals. The self-rocking mechanism enables the ~~rapid~~ redissolution of these salts into the feed, while Li^+ remains ~~stored~~ in the SPSE. Finally, Li^+ ions were eluted from the SPSE using 0.2 M HCl, yielding a Li^+-enriched solution (Figure S20). Li^+ concentration in the eluted solution reaches 27.5 $mg \cdot mL^{-1}$, which is 137 times higher than that in the original feed solution (Figure S21). Meanwhile, the concentration of competing ions decreases ~~significantly,~~ by several orders of magnitude. For instance, the concentration of Na^+ decreases from 11092 $mg \cdot mL^{-1}$ to 26.9 $mg \cdot mL^{-1}$.

After 30 regeneration cycles, the SPSE retained ~~excellent~~ adsorption performance, presenting a 21.6% decrease compared to its initial capacity, with a low Mn dissolution ratio of approximately 0.65% per cycle (Figure S22). The performance degradation ~~primarily~~ stems from the ~~inherent~~ instability of the ~~commercial~~ manganese-based lithium-ion sieve used in this work as a proof-of-concept. Future work could utilize more stable ~~commercial~~ titanium-based sieves to ensure improved cycling durability. ~~In addition,~~ The X-ray diffraction curves of SPSE indicates that the crystal structure of HMO remains stable after 30 cycle regenerations, which is attributed to relatively short elution time (Figure S23).

The scale-up potential of SPSE was assessed by assembling them into arrays for outdoor experiments (Figure S24-25). A total area of 0.024 m^2 SPSE was applied to extract Li^+ from 45 L of simulated seawater under natural sunlight over 12 days (Figure S26-27). ~~It is worth noting that~~ ~~i~~In the outdoor experiment, a higher liquid/solid (L/S) ratio (56.25 $L \cdot g^{-1}$) was used compared to the indoor experiment ~~(resulting in a more Li^+ content in the solution),~~ which is beneficial for simulating Li^+ extraction by SPSEs in large water bodies. The Li^+ concentration in the solution

Commented [A15]: Why is it more beneficial?

decreases to 35% of its initial value, and the equilibrium Li^+ adsorption reaches ~~approximately~~ 14.4 $mg \cdot g^{-1}$ **(Figure 5c)**. SPSE array achieves a higher adsorption capacity at a lower L/S ratio compared to literature~~s~~, indicating their higher Li^+ adsorption efficiency in seawater (Figure S28). The adsorption rate of the SPSE arrays over the eight days exceeds that of most previously reported HMO or HMO composite adsorbents (**Figure 5d** and Table S3). The eluted Li^+ was ~~further~~ precipitated into white Li_3PO_4 powder (Figure S29). ~~Additionally, t~~ Through further structural optimization, the SPSE-based device ~~successfully~~ achieved integrated water-lithium co-production, with the collected water maintaining high purity and meeting drinking-water quality standards (Figure S30-31 and Table S4-5).

In practical applications, SWRO brine is preferred as the Li^+ source for SPSE operation. Compared with natural seawater, SWRO brine ~~offers two key advantages: (1)~~ include pretreatment steps ~~involving~~ that ~~sterilization~~ sterilize and ~~impurity~~ remove impurities that may cause~~removal alleviate~~ biofouling, which can ~~and~~ extend the evaporator lifetime.~~; (2) the~~ The Li^+ concentration is ~~much~~ also higher in SWRO than that ~~in~~ of raw seawater. In addition, conducting Li^+ adsorption from SWRO brine on land ~~effectively avoids~~can avoid the influence~~s~~ of oceanic waves and currents, thereby expanding ~~the~~ its operational window and enhancing its durability. ~~The 12-day outdoor experiment further conforms the feasibility of SPSE in real-world conditions. In addition, w~~We provide a conceptual blueprint for integrating SPSE with existing RO plants (Figure S32), outlining a practical pathway toward sustainable Li^+ extraction from low-concentration brine streams.

Commented [A16]: Please spell out at first mention.

Commented [A17]: What is the cost of converting seawater to SWRO? The original selling point for this was to produce lithium from seawater. This paragraph may make the readers feel that they have been misled.

Commented [A18]: Seawater can be pumped on land, no?

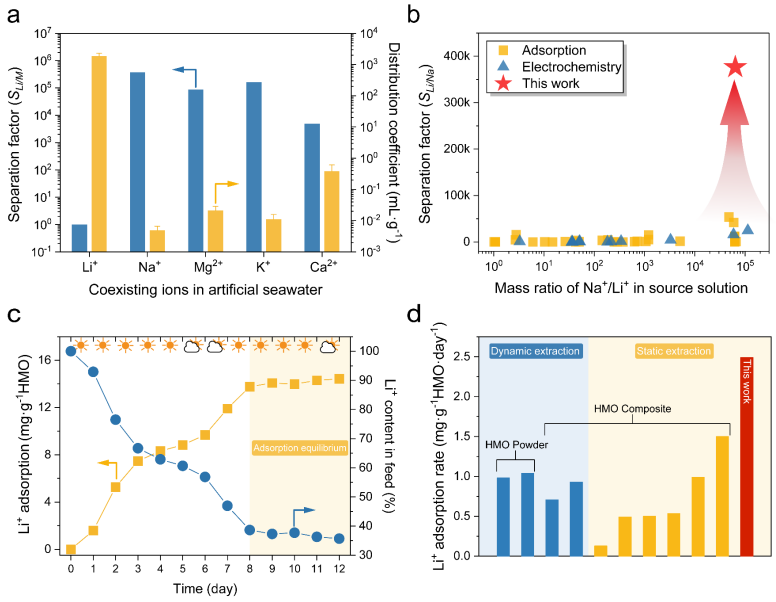

Figure 5. Selectivity and outdoor Li^+ extraction. (a) Separation factors and distribution coefficients of different ions within SPSE in simulated seawater. (b) Comparison of the Li^+/Na^+ separation factors among this work and previous literature. (c) Outdoor Li^+ adsorption of the SPSE arrays and variation of Li^+ content in feed over 12 days. The Li^+ concentration of simulated seawater is 0.2 mg·L^{-1}. (d) Comparison of Li^+ adsorption rates among this work and reported HMO-based adsorbents applied to seawater.

Conclusion and Outlooks

~~In summary,~~ W~~w~~e ~~have~~ designed an SPSE to achieve efficient and selective Li^+ extraction from seawater. In the seesaw configuration, ions ~~can~~ are~~be~~ continuously pumped into the SPSE by the evaporation-induced capillary flow, and the increasing local Li^+ concentration drives continuous diffusion and adsorption within the SPSE, overcoming sluggish adsorption kinetics caused by the

~~extremely~~ low Li^+ concentration. ~~Concurrently,~~ T~~t~~he self-descaling capacity allows the SPSE to re-dissolve salt scaling from competing ions into the bulk solution while Li^+ ions are captured ~~exclusively~~. ~~Consequently,~~ ~~t~~The SPSE achieved a high Li^+ adsorption of 14.43 $mg \cdot g^{-1}$ in simulated seawater under natural conditions with a Li^+/Na^+ separation factor surpassing 370,000. ~~This design offers a novel pathway for efficiently extracting Li^+ from trace Li^+ containing water bodies like seawater.~~

~~Experimental Section~~METHODS

Preparation of SPSEs

HMO/PAN nanofibers were constructed by electrospinning. Briefly, 15 wt% HMO nanoparticles were dispensed in DMF and then 15 wt% PAN powder was dissolved into the solution under stirring at 80 °C. The mixed solution was used for electrospinning at the feeding rate of 0.8 $mL \cdot h^{-1}$ under a voltage of 14 kV for 2 h. Subsequently, the loose nanofibers were folded and thermo-compressed at 0.5 MPa for 5 minutes to obtain the mat. 15 wt% PAN solution was blade-coated on carbon paper as a binder. The carbon paper was pasted on both sides of the mat and transferred to an aqueous solution for the phase transition of binder. Glass fiber with a diameter of 0.5 mm was attached to the center of the SPSE as the pivot.

Solar-powered solution supply

Before testing, the dry SPSE was placed at a specified tilt angle in a solution-filled container for 30 minutes to reach capillary transport equilibrium. Subsequently, only the SPSE was exposed to one-sun irradiation (xenon lamp equipped with an AM 1.5G filter, CEL-HXF300-T3), whereas the container was wrapped around with expanded polystyrene foam. The mass change of the solution

Commented [A19]: Please add another 200 words to discuss the limitations of this device (1) compared to competitors and (2) when used in the real world and (3) what is needed for deployment, e.g. regarding durability, cost, etc. Please give specific directions for each.

Formatted: Normal

was monitored using an electronic balance. Under illumination, the solar-powered solution supply (u) results from capillary-driven internal flow, which is considered equivalent to the evaporation rate ($\dot{m}$) calculated by the following equation:

$$u = \dot{m} = \frac{\Delta m}{\Delta t} \quad (3)$$

where Δm is the constant mass change (kg), Δt is the evaporation time (h). It should be noted that Δm used in the calculation was obtained under steady-state evaporation.

Li^+ extraction

To simulate the seawater reverse osmosis brine, 7 wt% NaCl solution was prepared with varying Li^+ concentrations, and the pH was adjusted to 11 by NaOH. The SPSE was floated on the feed solution (90 mL) with a liquid-to-solid (L/S) ratio of 6.75 $L \cdot g^{-1}$ under simulated one-sun irradiation (xenon lamp equipped with an AM 1.5G filter, CEL-HXF300-T3) with controlled environmental conditions (Temperature: 25 ± 2 ℃, relative humidity: 50 ± 10%). The mass change of the solution was monitored using an electronic balance and the metal ion concentration of the solution was detected by ICP-MS. Li^+ adsorption was estimated by adsorption capacity (q_e, $mg \cdot g^{-1}$) which is defined as follows:

$$q_e = \frac{C_0 \times V_0 - C_e \times V_e}{m} \quad (4)$$

where C_0 and C_e are the initial and equilibrium concentrations ($mg \cdot L^{-1}$) of Li^+, V_0 and V_e are the initial and equilibrium volume (L) of the solution, m is the mass of HMO in the SPSE (g).

The ion enrichment

The ion enrichment degree is defined as the ratio of the final salt concentration (ω_{final}) to the initial concentration ($\omega_{initial}$).

$$\text{Ion enrichment} = \frac{\omega_{final}}{\omega_{initial}} \quad (5)$$

Salt concentration data was obtained by cutting some area of the SPSE and followed with measuring the total amount of salt. Prior to test, the masses of both the dried SPSE (m_{dry}) and the SPSE after reaching capillary transport equilibrium ($m_{wetting}$) were recorded. After operation under solar irradiation for a specified period, the SPSE was removed from the evaporation system and cut into multiple samples. Each sample was recorded by digital imaging for area calculation using Image J software. The samples were then oven-dried overnight and subsequently immersed in 5 mL of deionized water for more than 12 hours with continuous shaking. The concentration of the leaching solution (C) was then determined using a conductivity meter (FE32-Standard, Mettler Toledo). The final salt concentration (ω_{final}) can be calculated as below:

$$\omega_{final} = \frac{C \times V}{A \times (\frac{m_{wetting} - m_{dry}}{A_0})} \quad (6)$$

Where C is the NaCl concentration of the leaching solution (mg·mL^{-1}), V is the volume of the leaching solution (mL), A is the area of the sample (cm^2), A_0 is the area of SPSE (cm^2), m_{dry} and $m_{wetting}$ are the weight of SPSE before and after wetting (mg), respectively.

Selectivity within SPSE

To verify selectivity within the SPSE, commercial sea salt was dissolved in DI water to gain simulated seawater, and the pH value was adjusted using NaOH. The initial concentrations of Li^+, Na^+, Mg^{2+}, K^+, and Ca^{2+} were 0.2, 11092, 849, 559 and 444 mg·L^{-1}, respectively. Notably, unlike traditional adsorption, Li^+ adsorption occurs within the SPSE, rather than in the bulk solution. It is necessary to obtain the ion concentration inside the SPSE after Li^+ adsorption. Before testing, the SPSE needed to be weighed in both dry and wet states to determine the amount of solution within the SPSE. Subsequently, after adsorbing for 10 h under light, the SPSE was transferred to an oven of 80 °C overnight to remove the solvent. The SPSE containing salt crystals was immersed in 100 mL of DI water for 24 h to fully dissolve the salt crystals, obtaining the internal ion concentration.

Finally, the SPSE was multiple rinsed and followed by desorption using 0.2 M HCl. The distribution coefficient (K_d) is a parameter that characterizes adsorption performance, defined as the ratio of the equilibrium adsorption capacity of Li^+ on the adsorbent to their equilibrium concentration in solution. Separation factor ($S_{Li/M}$) is defined as the ratio of the distribution coefficient of the target ion to that of the competing ion, and it is commonly employed to assess the selectivity of the adsorbent. The specific calculation formulas are as follows:

$$K_d = \frac{qe}{C_e} \quad (7)$$

$$S_{Li/M} = \frac{K_d(Li)}{K_d(M)} \quad (8)$$

where qe represents the adsorption capacity of the adsorbent at equilibrium ($mg \cdot g^{-1}$), and C_e denotes the equilibrium concentration of ions in solution ($mg \cdot L^{-1}$).

Outdoor experiment

The outdoor experiment was conducted in the Zijingang Campus of Zhejiang University (30°30' N, 120°08' E). The array consisting of 60 SPSE units extracted Li^+ from 45 L simulated seawater (pH = 11, Li^+ concentration = 0.2 $mg \cdot L^{-1}$, L/S ratio = 56.25 $L \cdot g^{-1}$) under natural sunlight. The variations in temperature and humidity, solar irradiance and mass change within days were recorded by a digital temperature-humidity recorder, a solar power meter and a platform balance, respectively. After the extraction, the SPSE arrays underwent multiple rinses and desorption using 0.2 M HCl. The pH value of the concentrated solution was adjusted to 12 by 0.2 M NaOH, following the filtration of the precipitate. Finally, lithium phosphate (Li_3PO_4) precipitated after the addition of Na_3PO_4.

~~**Supporting Information.**~~ **RESOURCE AVAILABILITY**

Lead Contact

Material Availability

Data and Code Availability

~~The following files are available free of charge.~~

Materials and methods; Detailed characterizations of SPSEs; Time-dependence fold enrichment within the SPSEs; Li^+ adsorption kinetics and long-term stability of SPSEs with and without self-rocking; Desorption kinetics and ion concentration in desorption solution of the SPSE after Li^+ extraction; Reusability of the SPSE. Detailed characterizations of SPSE arrays; The outdoor extraction experiment. (PDF)

Commented [A20]: Please fill out this section.

Formatted: Normal, Space After: 0 pt

Commented [A21]: Information here should be moved/included in the resource availability section.

Corresponding Author

*Hao-Cheng Yang: yanghch@zju.edu.cn

*Seth B Darling: darling@anl.gov

*Zhi-Kang Xu: xuzk@zju.edu.cn

Author Contributions

Conceptualization: Y-Z. Chen, H-C. Yang, Z-K. Xu. Methodology: Y-Z. Chen, H-N. Li. Investigation: Y-Z. Chen, H-N. Li, J-H. Xin, L-S. Wan. Data Curation: Y-Z. Chen, H-N. Li, J-H. Xin. Visualization: Y-Z. Chen. Supervision: H-C. Yang, Z-K. Xu, S-B. Darling. Writing-review and editing: All authors have participated. The manuscript was written through the contributions of all authors. All authors have approved the final version of the manuscript.

Funding Sources

Financial support for this work was provided by the National Natural Science Foundation of China (U21A20300) and Natural Science Foundation of Zhejiang Province (LZ25E030004). Work by SBD was supported as part of the Advanced Materials for Energy-Water Systems (AMEWS) Center, an Energy Frontier Research Center funded by the US Department of Energy, Office of Science, Basic Energy Sciences at Argonne National Laboratory under contract DE-AC02-06CH11357.

Acknowledgment

Financial support for this work was provided by the National Natural Science Foundation of China (U21A20300) and Natural Science Foundation of Zhejiang Province (LZ25E030004). Work by SBD was supported as part of the Advanced Materials for Energy-Water Systems (AMEWS) Center, an Energy Frontier Research Center funded by the US Department of Energy, Office of Science, Basic Energy Sciences at Argonne National Laboratory under contract DE-AC02-06CH11357.

METHODS

Materials

Lithium manganese oxide (LMO) particles were obtained from Shanghai Deepak Biotechnology Co., Ltd. Hydrogen manganese oxide (HMO) particles were prepared by dispersing LMO in 0.5M HCl for 24 hours. Lithium chloride (LiCl) was obtained from Shanghai Aladdin Reagent Co., Ltd. Dimethyl Formamide (DMF), hydrochloric acid (HCl) sodium chloride (NaCl), sodium hydroxide (NaOH) and sodium phosphate (Na_3PO_4) were obtained from Sinopharm Chemical Reagent Co., Ltd. Polyacrylonitrile powder (PAN, Mn = 80000) was obtained from China Petrochemcial Co., Ltd. Anqing Branch. Carbon paper and sea salt were commercially sourced products. Deionized (DI) water was produced by an ELGA LabWater system (France). All chemicals were utilized without further purification.

Commented [A22]: Methods moved from the supplementary document to the main text as required.

Commented [A23]: This should be moved up to combine with the existing methods section.

Formatted: Font: 16 pt, Bold

Formatted: Font: 16 pt, Bold

Characterization

Surface morphologies of PAN/HMO nanofibers were observed using a field emission scanning electron microscope (FE-SEM, TM3030Plus, HITACHI, Japan) and a transmission electron microscopy (TEM, HT-7700, HITACHI, Japan). The metal ion concentrations were detected by inductively coupled plasma-mass spectrometry (ICP-MS, NexION 300X, PerkinElmer, USA). The crystalline structure of nanoparticles and lithium phosphate was obtained through the X-Ray diffractometer (XRD, D8 ADVANCE, Bruker, Germany). The transmission and reflection spectra were measured by using an ultraviolet-visible-near-infrared spectrophotometer (UV-vis-NIR, UH4150, HITACHI, Japan). The water contact angles were measured using an Optical Surface Analyzer-100 system (Ningbo NB Scientific Instruments Co., Ltd, China). The forces for rocking were evaluated by a microbalance system on the dynamic contact angle analyzer (Data-physics, DCAT25, Germany). The porosity and permeability of PAN/HMO nanofibers were determined using a mercury porosimeter (AutoPore IV 9510, USA). HMO content PAN/HMO nanofibers was determined by thermogravimetric analysis (TGA, TA Q50, USA).

Monitoring of salt mass on the SPSE

We designed a dual-balance experimental apparatus containing a jib crane structure to simultaneously monitor changes in salt mass and bulk solution. The test solution consists of a 7 wt% NaCl solution (90 mL). The mass of the dry SPSE is 0.45 g ± 0.1 g, while the mass after saturation with water is 1.10 g ± 0.20 g. A schematic of the experimental setup is shown in **Figure S26**. The pivot of the SPSE is suspended by the jib crane on the Balance 1, ensuring it remains suspended and does not contact the container. A syringe pump is used to replenish the solution in the container, compensating for vapor losses and preventing changes in the liquid level that could alter the force distribution on the SPSE. During the evaporation process, the variation in the left balance corresponds to changes in the salt mass on the SPSE.

Numerical simulation

The calculation and analysis of the ion distribution within the SPSE are carried out via COMSOL Multiphysics 6.1. The SPSE is modeled at a 1:1 scale corresponding to the actual device. Experimental data provides the initial values and boundary conditions for this simulation. The flow of water inside the device is characterized using the Brinkman equation, which is as follows:

Commented [A24]: Please give a more descriptive title here.

$$\frac{1}{\varepsilon_p}\rho\frac{\partial \mathbf{u}}{\partial t}=\nabla\cdot\left[-p\mathbf{I}+\mathbf{K}\right]-\left(\mu\kappa^{-1}+\beta\rho|\mathbf{u}|+\frac{Q_m}{\varepsilon_p^2}\right)\mathbf{u}+\mathbf{F}+\rho\mathbf{g}$$

Field Code Changed

In the equation, ε_p is the porosity of the porous medium (0.7722, determined by mercury intrusion method), $\boldsymbol{u}$ is the velocity vector of the fluid, ρ is the density of the fluid, μ is the dynamic viscosity of the fluid, p is the pressure, κ is the permeability of the porous medium (1.713×10^{-12} m^2, determined by mercury intrusion method), Q_m is a mass source or sink and $\boldsymbol{F}$ is a force term to account for the influence of gravity and other volume forces. $\boldsymbol{K}$ is described by the following expression:

$$\mathbf{K}=\mu\frac{1}{\varepsilon_p}\left(\nabla\mathbf{u}+(\nabla\mathbf{u})^T\right)-\frac{2}{3}\mu\frac{1}{\varepsilon_p}(\nabla\cdot\mathbf{u})\mathbf{I}$$

Field Code Changed

The concentration variations in the system are described in detail by the convection-diffusion equation. The transportation of LiCl is characterized by the transport of concentrated species, which is as follows:

$$\rho\frac{\partial \omega_i}{\partial t}+\nabla\cdot\mathbf{j}_i+\rho(\mathbf{u}\cdot\nabla)\omega_i=R_i$$

Field Code Changed

where ω_i is the mass fraction of the species, $\boldsymbol{j}_i$ is the diffusive flux vector, R_i is the net reaction rate of species. The ions diffuse in the device due to the existence of a concentration gradient. In the simulation, the diffusion coefficient is 2.67×10^{-9} $m^2 \cdot s^{-1}$. The mass fractions of LiCl and H_2O are 4×10^{-4} and 999.9996 $mol \cdot m^{-3}$.

The calculation couples flow and species transport together to represent the LiCl distribution in the SPSE.

Torque equilibrium model

To quantitatively evaluate the adhesive force between the water and SPSE, a metal rod connected to a microbalance system was used to apply a controlled vertical displacement to the SPSE. The microbalance continuously recorded the variation in the net resisting force prior to flipping, with a stepwise displacement rate of 10 $mm \cdot min^{-1}$. As shown in Figure S10, when the SPSE was submerged below the liquid surface, the adhesive force increased linearly with displacement. In this regime, the measured force comprises the combined contributions from the liquid bridge adhesion, buoyancy, and surface tension acting on the hydrophobic layer. Once the SPSE moved above the liquid surface, only the liquid bridge adhesion remained, and this force increased nonlinearly with displacement. Therefore, we identified the critical flipping point as being dominated by the adhesive force originating from the liquid bridge.

A liquid bridge forms a meniscus of liquid between two solid surfaces. The total capillary force (F_c) generated by such a bridge consists of two components: a surface-tension term (arising from the curved liquid–air interface) and a pressure-difference term (arising from the Laplace pressure

across the meniscus). The total force can thus be expressed as:

$$F_c = 2\pi r\gamma\cos\theta + \pi r^2 \Delta P$$

where γ is the surface tension of the liquid (N·m^{-1}), r is the radius of the liquid bridge (m), θ is the contact angle, and ΔP is the Laplace pressure difference given by:

$$\Delta P = \gamma\left(\frac{1}{r_1} + \frac{1}{r_2}\right)$$

where r_1 and r_2 are the principal radii of curvature of the liquid meniscus. When approaching the flipping transition, r_1 and $r_2 \gg r$, and thus the Laplace pressure term becomes negligible. In this limit, the capillary force can be simplified to:

$$F_c \approx 2\pi r\gamma\cos\theta$$

The critical transition between the **static tilted (ion-enrichment)** state and the **dynamic rocking (self-descaling)** state occurs when the torque generated by salt accumulation on the suspended side surpasses the resisting torque from capillary adhesion. The rocking threshold is reached when the gravitational torque induced by the accumulated salt mass (m_{rock}) exceeds the adhesive torque from the liquid bridge, which can be expressed as:

$$m_{\text{rock}} = \frac{F_c}{g}$$

where g is the gravitational acceleration (9.81 m·s^{-2}).

Since the accumulated salt mass depends on the evaporation rate and the salt concentration of the solution, the flipping time (t_{rock}) can be expressed as:

$$t_{\text{rock}} = \frac{m_{\text{rock}}}{RAC_0}$$

where R is the evaporation rate (kg·m^{-2}·s^{-1}), A is the effective evaporation area (m^2), and C_0 is the salt concentration (wt%). This formulation quantitatively links the rocking dynamics of the SPSE to the coupled processes of capillary adhesion and evaporation-driven salt accumulation.

References

Commented [A25]: These two parts may fit in the supplementary document (or here, up to you). If you want to move this to the supplementary document, they will need a name and a title, i.e. Note S1: Numerical simulation of ion distribution in the SPSE, etc.
And the note must be cited in the main text as Note S1, for example.

Formatted: Normal

[1] A.Z. Haddad, L. Hackl, B. Akuzum, G. Pohlman, J.-F. Magnan, R. Kostecki, How to make lithium extraction cleaner, faster and cheaper - in six steps. *Nature* **616**, 245-248 (2023).

[2] M. L. Vera, W. R. Torres, C. I. Galli, A. Chagnes, V. Flexer, Environmental impact of direct lithium extraction from brines. *Nat. Rev. Earth Environ.* **4**, 149-165 (2023).

[3] IEA, Total lithium demand by sector and scenario, 2020-2040, (2021); https://www.iea.org/data-and-statistics/charts/total-lithium-demand-by-sector-and-scenario-2020-2040

[4] H. Bae, Y. Kim, Technologies of lithium recycling from waste lithium ion batteries: a review. *Mater. Adv.* **2**, 3234-3250 (2021).

[5] Y. J. Lim, K. Goh, A. Goto, Y. Zhao, R. Wang, Uranium and lithium extraction from seawater: challenges and opportunities for a sustainable energy future. *J. Mater. Chem. A* **11**, 22551-22589 (2023).

[6] S. Yang, Y. Wang, H. Pan, P. He, H. Zhou, Lithium extraction from low-quality brines. *Nature* **636**, 309-321 (2024).

[7] Kazi, W. Chen, J. G. Eatman, F. Gao, Y. Liu, Y. Wang, Z. Xia, S. B. Darling, Material Design Strategies for Recovery of Critical Resources from Water. *Adv. Mater.* **35**, 2300913 (2023).

[8] Liu, Y. Li, D. Lin, P.-C. Hsu, B. Liu, G. Yan, T. Wu, Y. Cui, S. Chu, Lithium extraction from seawater through pulsed electrochemical intercalation. *Joule* **4**, 1459-1469 (2020).

[9] K. Sun, M. Tebyetekerwa, X. Zeng, Z. Wang, T. T. Duignan, X. Zhang, Understanding the electrochemical extraction of lithium from ultradilute solutions. *Environ. Sci. Technol.* **58**, 3997-4007 (2024).

[10] H. Peng, X. Liu, Y. Su, J. Li, Q. Zhao, Advanced lithium extraction membranes derived from tagged-modification of polyamide networks. *Angew. Chem. Int. Ed.* **62**, e202312795 (2023).

Commented [A26]: The main reference list (and any supplemental reference list) should be numbered and formatted according to

[11] Z. Zhou, J. Fan, X. Liu, Y. Hu, X. Wei, Y. Hu, W. Wang, Z. Ren, Recovery of lithium from salt-lake brines using solvent extraction with TBP as extractant and $FeCl_3$ as co-extraction agent. *Hydrometallurgy* **191**, 105244 (2020).

[12] Weng, H. Duan, Y. Hou, J. Huo, L. Chen, F. Zhang, J. Wang, Introduction of manganese based lithium-ion sieve-a review. *Prog. Nat. Sci.: Mater. Int.* **30**, 139-152 (2020).

[13] X. Xu, Y. Chen, P. Wan, K. Gasem, K. Wang, T. He, H. Adidharma, M. Fan, Extraction of lithium with functionalized lithium ion-sieves. *Prog. Mater Sci.* **84**, 276-313 (2016).

[14] X. Chen, W. Yu, Y. Zhang, C. Huang, L. Nie, J. Yu, Y. Zhang, C. Zhang, W. Zhai, X. Zhang, Y. Yu, W. Liu, Solar-driven lithium extraction by a floating felt. *Adv. Funct. Mater.* **34**, 2316178 (2024).

[15] Q. Xia, Z. Deng, S. Sun, W. Zhao, J. Ding, B. Xi, G. Gao, C. Wang, Solar-enhanced lithium extraction with self-sustaining water recycling from salt-lake brines. *PNAS* **121**, e2400159121 (2024).

[16] H.-N. Li, C. Zhang, J.-H. Xin, Y.-W. Liu, H.-C. Yang, C.-Y. Zhu, C. Liu, Z.-K. Xu, Design of photothermal "ion pumps" for achieving energy-efficient, augmented, and durable lithium extraction from seawater. *ACS Nano* **18**, 2434-2445 (2024).

[17] K. Chen, L. Li, B. Li, Y. Yang, K. Zhu, J. Zhang, Simultaneous fresh water collection and Li^+ selective adsorption enabled by a salt-resistant separated solar evaporator. *Adv. Funct. Mater.* **34**, 2402221 (2024).

[18] Y. Song, S. Fang, N. Xu, M. Wang, S. Chen, J. Chen, B. Mi, J. Zhu, Solar transpiration–powered lithium extraction and storage. *Science* **385**, 1444-1449 (2024).

[19] S. B. Darling, The brine of the times. *Science* **385**, 1421-1422 (2024).

[20] L. Li, J. Zhang, Highly salt-resistant and all-weather solar-driven interfacial evaporators with photothermal and electrothermal effects based on Janus graphene@silicone sponges. *Nano Energ.* **81**, 105682 (2021).

[21] L. Li, K. Chen, J. Zhang, J. Zhang, Design of MOF-based solar evaporators with hierarchical microporous/nanobridged/nanogranular structures for rapid interfacial solar evaporation and fresh water collection. *ChemSusChem*, **17**, e202401224 (2024).

[22] J. M. Montanero, A. Ponce-Torres, Review on the dynamics of isothermal liquid bridges. *Appl. Mech. Rev.* **72**, 010803 (2019).

[23] J. Wang, X. Guo, Adsorption kinetic models: physical meanings, applications, and solving methods. *J. Hazard. Mater.* **390**, 122156 (2020).

[24] Kashchiev, *Nucleation : basic theory with applications*. (Oxford ; Boston : Butterworth Heinemann, 2000).

~~Table of Contents figure~~

~~This study presents a solar-powered seesaw extractor (SPSE) with a tri-layer architecture for Li^+ extraction from seawater. It harnesses sunlight to drive evaporation-induced capillary flow, enriching Li^+ concentrations by more than 15-fold within the adsorption layer and increasing Li^+ uptake by almost 70% over 120 hours compared to traditional methods.~~

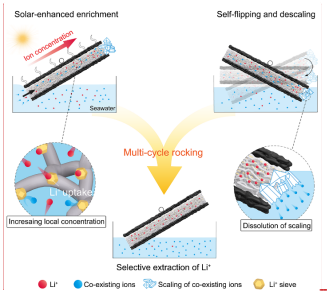

Commented [A27]: Please upload this as an individual file.